LAWRENCE
LIVERMORE
NATIONAL
LABORATORY

LLNL-PROC-755525

# Understanding tungsten divertor sourcing, SOL transport, and its impact on core impurity accumulation in DIII-D high performance discharges

D. M. Thomas, T. Abrams, C. J. Lasnier, M. A. Makowski, A. G. McLean, B. S. Victor

July 30, 2018

2018 EPS 45th Conf on Plasma Physics
Prague, Czech Republic
July 2, 2018 through July 6, 2018

## Disclaimer

# Understanding tungsten divertor sourcing, SOL transport, and its impact on core impurity accumulation in DIII-D high performance discharges *

D.M. Thomas[1], T. Abrams[1], J. Barton[2], J.A. Boedo[3], A.R. Briesemeister[4], D. Buchenhauer[2], I. Bykov[3], C.P. Chrobak[1], R. Ding[5], D. Donovan[6], J.D. Elder[7], B.A. Grierson[8], H.Y Guo[1], J. Guterl[4], E.T. Hinson[9], E.M Hollmann[3], C.J. Lasnier[10], A.W. Leonard[1], M.A. Makowski[10], A.G. McLean[10], R. Nygren[2], T.W. Petrie[1], D.L. Rudakov[3], P.C. Stangeby[7], E.A. Unterberg[4], B. Victor[10], W.R. Wampler[2], H.Q. Wang[4], J.G. Watkins[2], M. Zach[4]

[1]*General Atomics, General Atomics, San Diego, CA, USA*
[2]*Sandia National Laboratory, Albuquerque, NM, USA*
[3]*University of California San Diego, San Diego, CA, USA*
[4]*Oak Ridge National Laboratory, Oak Ridge, TN, USA*
[5]*Oak Ridge Associated Universities, Oak Ridge, TN, USA*
[6]*University of Tennessee, Knoxville, TN, USA*
[7]*University of Toronto, Toronto, ON, Canada*
[8]*Princeton Plasma Physics Laboratory, Princeton, NJ, USA*
[9]*University of Wisconsin, Madison, WI, USA*
[10]*Lawrence Livermore National Laboratory, Livermore, CA, USA*

Introduction - At present the use of tungsten as the plasma facing material (PFM) is foreseen at the strikepoints and far-target regions of divertors for next generation (e.g. ITER) tokamak reactor experiments. Because of the negative influence of even small core W concentrations on fusion performance [1], it is important to understand the sourcing and migration of W in thedivertor and scrape-off (SOL) region. The DIII-D Metal Rings Campaign was designed to address 3 key questions on the use of high-Z PFM by leveraging the predominantly low-Z environment on DIII-D: (i) how does tungsten source in the divertor region: i.e both at the strikepoint and far-target, (ii) how does W get transported to the core, and (iii) how does it affect the core performance. DIII-D offers a unique environment for these studies because of the lack of any preexisting tungsten in the vessel and the use of two toroidal rings of isotopically distinct W-coated tiles at two poloidal locations in the outer divertor.

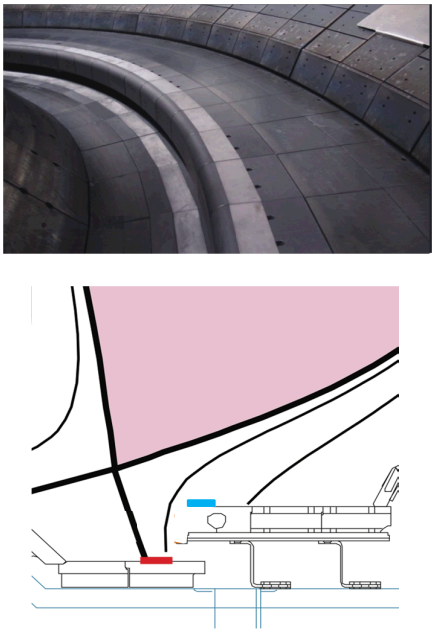

Figure 1: *(top) lower divertor of DIII-D, showing floor ring(left) and W-182 enriched shelf ring(right) (bottom) equilibrium schematic showing typical strikepoint and far SOL.*

Experimental Arrangement - The experiments used 5-cm wide rings of tungsten-coated molybdenum alloy (TZM)[2]. The lower 'floor' ring (R=1.32-1.37 m) was coated with natural isotopic abundance of stable W isotopes. The upper 'shelf' row (R=1.404-1.454 m) was coated with tungsten where the isotope W-182 was enriched from 26 at% up to 92.9 at%. Different plasma equilibria (LSN and DN) were employed to place the lower outer strike point on either one of

the rings, or between the two, to assess the dependence of sourcing, transport, and core concentration on strike point location and its proximity to the rings.

To determine the tungsten source intensity, gross erosion from each of the rings was estimated using the S/XB ratio and the W I intensity from filtered photodetectors, in conjunction with a survey spectrometer and local ($n_e$,$T_e$) estimates from divertor Thomson scattering and nearby Langmuir probes [3,4]. The apparatus is capable of resolving the inter-ELM and intra-ELM W flux. The SOL transport of W ions cannot be measured directly but is inferred on a shot-to-shot basis from the deposition profile of W on an ensemble of carbon collector probes inserted in the main SOL near the midplane [5]. Radial profiles of the deposited layers are analysed post-exposure using Rutherford backscattering and inductively-coupled plasma mass spectrometry. Because of the use of distinct isotopic mixtures, the relative contribution of each ring can be determined using this latter technique with a simple isotope mixing model [6]. The use of differing diameter collector probes provides measurements over a range of sampling volumes in the SOL. Finally, the core tungsten concentration is inferred from VUV and X-ray measurements of the $W^{45+}$ brightness in conjunction with STRAHL calculations constrained by radiated power profiles from bolometry and SXR tomography[7].

Results - In DIII-D ELMs source tungsten at many times the inter-ELM rate, with the source scaling with deposited energy [Figure 2]. The size of the ELM also influences the relative efficiency of transport of tungsten sputtered from the far target (representative of the divertor throat) compared to that sputtered at the strikepoint directly. This was investigated by placing the strikepoint on the inner ring with the far SOL on the outer ring, and normalizing the collected tungsten to the relative source strengths. With high-frequency small ELMs, tungsten transported from the strikepoint is dominant, with negligible transport of W-182 from the far-target [Figure 3]. However, with low frequency large ELMS, the far-target transport increases dramatically. This may be due to change in SOL turbulent transport during large ELMS as well as increased arcing [8] in the far-target region for larger ELMS which increases the relative W transport in the far SOL. The implication is that the relative contribution of divertor regions to upstream W SOL density is dependent on ELM size. Since the different diameter probes sample different lengths in the SOL both upstream and downstream of the probes, it is possible to draw some conclusions about the poloidal distribution of the W density in the outer-side main SOL.

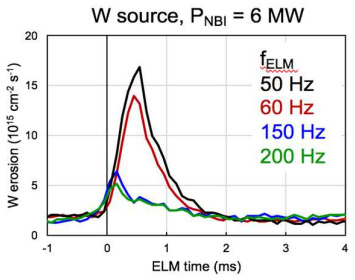


Figure 2: *W source rate for a variety of ELM frequencies.*

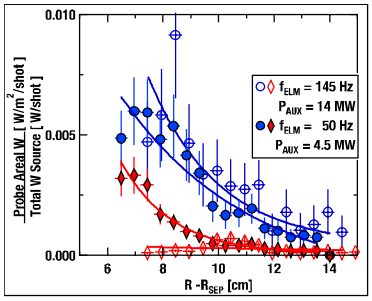


Figure 3: *Area density of W deposited on upstream collector probe originating from the strike point (blue) and far-target regions (red), normalized to source strength for high and low $f_{ELM}$ discharges.*

Fig 4 shows normalized W deposition profiles for a series of L-mode LSN discharges. For the smaller diameter probe having a sampling length $L_{COLL}$ ~ +/- 0.5-0.6 m, analysis of the OTF (outer target facing) and ITF (inner target facing) sides showed symmetric deposition profiles, indicating a uniform SOL concentration. In contrast, for the largest diameter probe ($L_{COLL}$ ~ +/- 4-10 m) there is a substantially larger deposit on the ITF side, despite the fact that the W-tile rings were in the outer divertor. These results may be explained by a W buildup in the SOL at the crown of the plasma (i.e., above the probe), driven by the balance of the parallel grad-$T_i$ and frictional forces. The larger probe samples this SOL region while the smaller probe does not [6]. The buildup and its rough poloidal location are consistent with OEDGE impurity transport modelling of these discharges [9] and support long-standing theoretical predictions about impurity transport in the divertor and SOL[10].

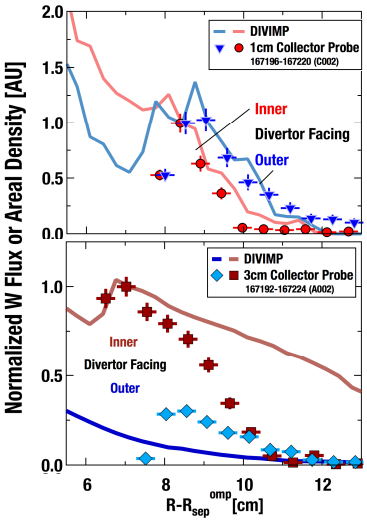


Figure 4: *Upstream and downstream W deposition profiles for probes having different poloidal collection lengths.*

The compatibility of DIII-D Advanced Tokamak operation with the use of W in the divertor was also investigated. The radial location of the ECCD appears to be a key factor in maintaining good AT performance. In the case of a steady state hybrid scenario with $q_0$~1 with the strike point on the ring, the use of on-axis ECCD was successful in mitigating the accumulation of W in the core and $\beta_n$ and energy confinement were equivalent to those of an all-carbon divertor shot [Figure 5], with no increase in core radiation. In contrast, for a higher $q_{min}$ ($q_0$ ~ 1.7) scenario where off axis ECCD is used to broaden the current profile, enhanced core W buildup and excessive core radiation lead to a drop in both $\beta_n$ and confinement [11]. The difference in the core radiation profiles, obtained from bolometric inversion is shown in Figure 6.

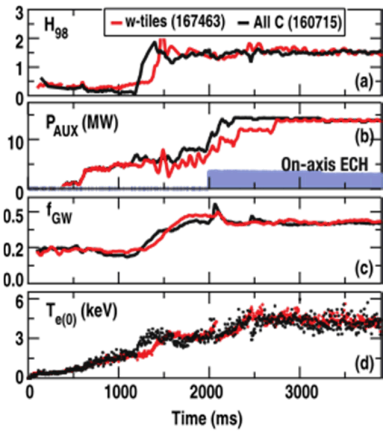


Figure 5: *Comparison of AT discharge with (red) and without (black) W divertor inserts. a) H-factor; b) total injected power, $P_{AUX}$; c) Greenwald fraction, $f_{GW}$; and d) central electron temperature, Te(0).*

<u>Conclusions</u> - Targeted diagnostics and isotopically distinct W rings have been used to understand localized divertor W sourcing and SOL transport in DIII-D discharges. Consistent with earlier JET studies [12], high performance plasmas have been successfully run with tungsten at the outer divertor strike point with on-axis electron heating. However this presently depends on the enhanced impurity transport due to central

ECH to achieve adequate W concentration control. In the future, we plan to install additional W rings at different poloidal locations in the new Small Angle Slot Divertor [13] to study the advantage of this type of slot divertor with respect to impurity retention and core performance.

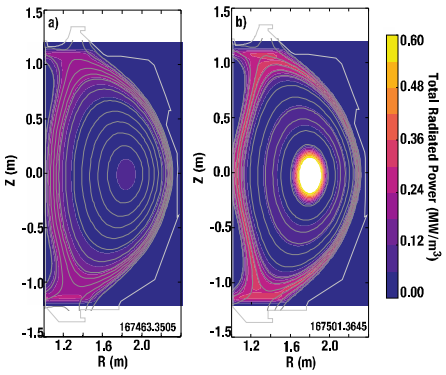


Figure 6: *Comparison of radiated power profiles for (a) standard DIII-D hybrid AT and (b) high $q_{min}$ hybrid AT scenarios.*

Acknowledgements - This work was performed in part under the auspices of the U.S. Department of Energy by General Atomics under DE-FC02-04ER54698, DE-FG02-07ER54917, DE-AC05-00OR22725, DE-NA0003525, DE-AC0209CH11466, DE-AC52-07N27344, and DEAC05-00OR23100. DIII-D data shown in this paper can be obtained in digital format by following the links at https://fusion.gat.com/global/D3D_DMP. 

## References

[1] Putterich T *et al., 2010 Nuclear Fusion **50**, 025012*
[2] Holtrop K et al, *2017 Fusion Sci Technol 72:4*
[3] Abrams T, et al., *2017 Nucl. Fusion **57** 056034*
[4] Abrams T, et al., *2018 IEEE T. Plasma Sci. **46** 1298*
[5] Stangeby P ,*1987 Physics of Fluids **30**, 3262*
[6] Donovan D, et al. 2018, submitted *RevSci Instrum*
[7] Victor B, et al. *2017 EPS*
[8] Bykov, I et al. *2017 Phys. Scr. **T170**, 014034*
[9] Elder D. *et al. 2018 PSI*
[10] Neuhauser J, *et al. 1984 Nuclear Fusion* **24**, 39
[11] Victor B. *et al., 2017 APS*
[12] Angioni, *et al., 2014 Nuclear Fusion **54**, 083028*
[13] Guo H, *et al., 2017 Nucl. Fusion **57** 044001, and 2017 APS*